Phys. Status Solidi A **210,** No. 5, 1025–1029 (2013) / **DOI** 10.1002/pssa.201200737

physica status solidi a
www.pss-a.com
applications and materials science

Part of Special Section on
Engineering of Functional Interfaces

A combinatorial properties study of thin film Al–Fe alloys

Andrei I. Mardare and Achim Walter Hassel*

Institute for Chemical Technology of Inorganic Materials, Johannes Kepler University, Altenberger Str. 69, 4040 Linz, Austria

Received 18 September 2012, revised 10 October 2012, accepted 22 October 2012
Published online 18 February 2013

Keywords anodic oxide films, combinatorial libraries, scanning droplet cell microscopy, X-ray photoelectron spectroscopy

* Corresponding author: e-mail achimwalter.hassel@jku.at, Phone: +43 732 2468 8700, Fax: +43 732 2468 8905
Web: www.jku.at/ictas

The microstructure of an Al–Fe combinatorial thin film library with a compositional spread ranging from 5 to 23 at.% Fe was analysed. The local crystallographic properties were correlated to the film microstructure dynamic changes. The presence of a transitional region between two metastable phases in the Al–Fe alloys was identified and related to a percolation threshold near Al-12 at.% Fe. Anodic oxidation of the parent metals produced a mixed oxide on the surface of the Al–Fe library. XPS investigation of the mixed oxides suggested an intimate mixing of Al_2O_3 and Fe_2O_3.

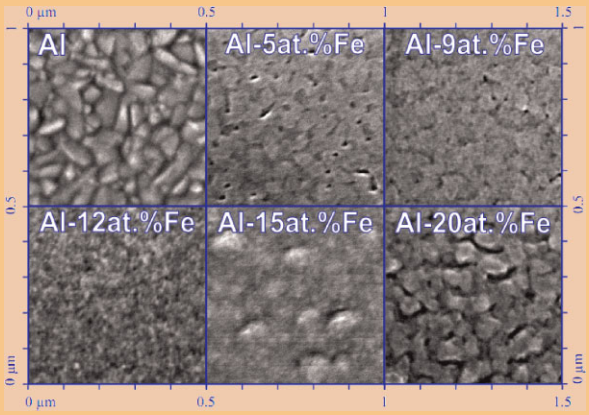

1 Introduction Nanocrystalline alloys with grain sizes below 100 nm have received increased scientific interest due to various mechanical, tribological, and magnetic applications where they showed superior performances as compared to microsized grain structures. The mechanical properties of electron beam deposited Al–Fe alloys with Fe contents below 2 at.% have been studied by Mukai et al. [1]. Unique mechanical properties materialised in abnormally high tensile strengths were assigned to nanometer-sized subgrains along with a high angle grain structure. Sputter deposited Al–Fe alloy films containing 4 at.% Fe or 7.5 at.% Fe were anodised in an ammonium pentaborate solution [2, 3]. Iron from the matrix accumulated in a 2–3 nm thick sublayer of near Al_3Fe composition rather that being incorporate in the oxide.

High dose high energy implantation of Fe into Al initially forms the intermetallic disordered phase Al_5Fe_2 that converts during annealing at 630 °C for 1 h into an intermetallic compound with lower Fe content of the nominal composition $Al_{13}Fe_4$ of rod shaped micrometer-sized structure [4].

A number of studies show that the properties of a material decisively depend not only on the composition but also on the microstructure. For Al–Cu alloys for example the dispersoid intermetallics showed the highest activity, an effect that significantly influences the corrosion resistance of Al alloys [5]. A combinatorial study with a composition spread on the other hand showed that aluminium stays passive over a wide range of composition and only when a certain threshold is exceeded, the alloy shows a more active behaviour through oxygen evolution [6]. Iron behaves in a similar way as copper and was also studied in a composition spread. Interestingly an unpredicted singularity was observed for this material library, in which the onset potential of anodisation was shifted to higher values in a very narrow range between 9 and 12 at.% Fe [7]. In an attempt to further elucidate this behaviour the present work presents a detailed study of the microstructural effects in an

aluminium iron material library with Fe contents from 5 to 23 at.%.

2 Experimental techniques In the present work, a graded Al–Fe sample was co-deposited from vapour phase using a thermal co-evaporation system operating in a vacuum chamber with a base pressure of 2×10^{-4} Pa. Silica microscope slides were used as substrate. Two thermal evaporation sources were used simultaneously for the evaporation of high purity (99.999%, Goodfellow) Al and Fe at room temperature, with deposition rates of 1 and 0.5 nm s^{-1}, respectively. This ensured a vapour phase mixed Al–Fe solid solution formation on the surface of the substrate. The final thickness of the graded Al–Fe thin film was approximately 100 nm. The co-evaporation setup and the sample preparation are described in detail elsewhere [7].

Energy dispersive X-ray spectroscopy (EDX – INCA software) was used for mapping the component concentrations along the sample. An Fe concentration variation from 5 to 23 at.% was measured, which corresponds to a linear composition gradient of 2.57 at.% cm^{-1}. The surface morphology of the Al–Fe thin film combinatorial alloys was imaged using scanning electron microscopy (SEM) at various concentrations. X-ray diffraction analysis (XRD) was used for the characterisation of crystallographic orientations of the metallic co-deposits along the Al–Fe compositional spread. Due to the small thickness of the Al–Fe thin film, a grazing incidence angle (1°) was used for minimising the substrate absorption, enhancing the surface diffraction in the thin film.

A borosilicate capillary-based scanning droplet cell microscope (SDCM) [8] with a tip diameter of 200 μm was involved in the mapping of the surface properties of the Al–Fe combinatorial library. A capillary reference electrode μ-AuHg/$Hg_2(CH_3COO)_2$/$Na(CH_3COO)$ having a 100 μm tip diameter was used [9]. A 1 mm wide Au band that was wrapped around the reference electrode capillary acted as counter electrode. The advantage of the small area under investigation was combined with a fully automatic scanning system capable of investigating the Al–Fe compositional spread with a resolution of 1 at.%. Details about the SDCM fabrication and automation can be found elsewhere [10, 11].

An acetate buffer solution was used as electrolyte and the open circuit potential (OCP) of the surface of Al–Fe combinatorial alloys was mapped using an equilibration time of 150 s. In a second scan on the Al–Fe alloys, the applied potential of the SDC was increased anodically at a rate of 100 mV s^{-1} up to a maximum of 10 V. Surface analytical investigations, by means of X-ray photoelectron spectroscopy (XPS), were done on the surface of anodic oxides grown at maximum potential for various concentrations of the parent metal alloys.

3 Results and discussion The microstructure of various Al–Fe alloys is presented in Fig. 1. On a pure Al thin film, evaporated under similar conditions as the combinatorial library, small grains can be observed forming a compact surface with distinctly visible grain boundaries.

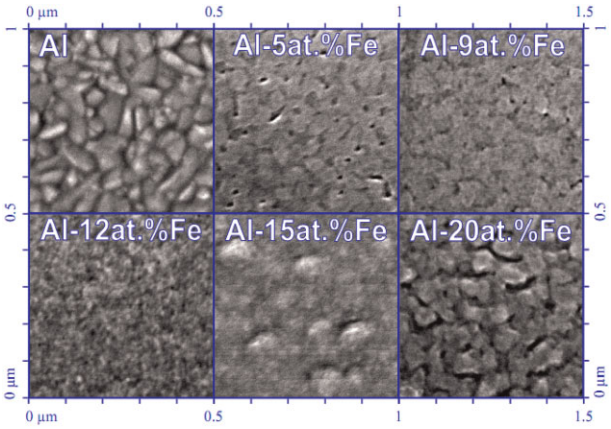

Figure 1 (online colour at: www.pss-a.com) SEM images of the Fe–Al graded sample at different concentrations together with the surface of a pure Al thin film.

Addition of small amounts of Fe in the thin film for Al–Fe alloys leads to a flattening of the metallic grain structures as observed for 5 and 9 at.% Fe. The microstructure continuously changes with the increase of Fe concentration and no surface features can be observed for Al-12 at.% Fe. The grains start to reform at Al-15 at.% Fe and the surface morphology becomes again stable for Fe concentrations higher than 20 at.%, where individual grains can be observed together with small intergranular voids with widths of around 20 nm. The microstructure evolution of the metallic alloys suggests the presence of a threshold around the composition of Al-12 at.% Fe in the Al–Fe combinatorial library. This can be attributed to a change between two different metastable crystallographic phases, since the Al–Fe equilibrium phase diagram does not show any particular phase boundaries for this concentration [12].

Several X-ray diffractograms measured for alloys with different Fe contents are presented in Fig. 2. The XRD measured on a pure Al thin film and the positions of the α-Fe main orientation peaks are shown as references. The increased background level at small angles is due to the small thickness of the metallic films (100 nm). Nevertheless, the presence of the (220) diffraction plane corresponding to the fcc structure of pure Al can be observed in the alloys for Fe concentrations up to 15 at.%, while the (110) plane, corresponding to the bcc structure of pure α-Fe, starts to diffract at compositions of Al-10 at.% Fe and above. However, since both Al (220) and Fe (110) orientations are so close to each other, the broadening of the diffraction peak may be due to the coexistence of both materials. The presence of a threshold for Fe concentrations between 10 and 15 at.% can be observed, suggesting a crystallographic transition between fcc and bcc structures in the Al–Fe combinatorial library. The surface modifications observed in Fig. 1 confirm this structural change and the transition is visualised in a zone with no visible features at Al-12 at.% Fe

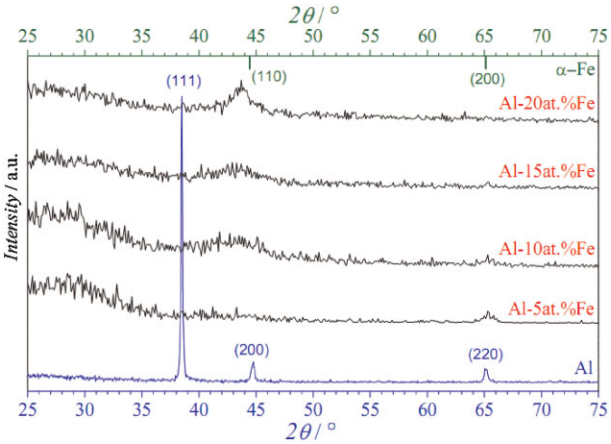

Figure 2 (online colour at: www.pss-a.com) XRD spectra measured for different alloys in the Al–Fe compositional spread together with the crystallographic orientations of a pure Al thin film.

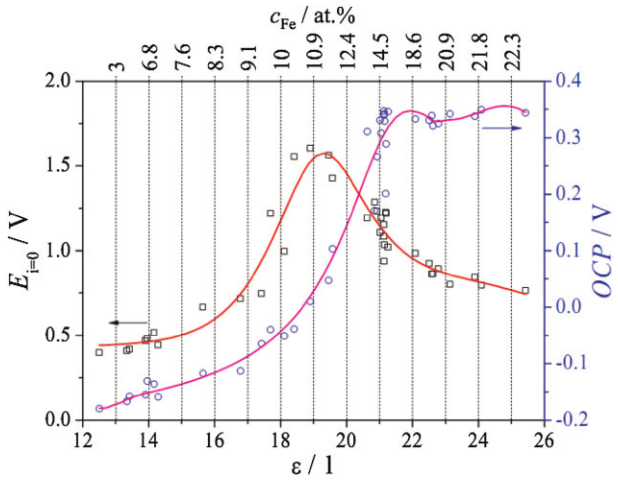

Figure 3 (online colour at: www.pss-a.com) Zero current and OCPs of the Al–Fe alloys mapped along the compositional gradient and dielectric constant variation of the mixed anodic oxide.

probably due to rearranging of the crystallographic lattices. The XRD analysis confirmed that a metallic solid solution was obtained using this co-deposition method and no hints of the formation of Al–Fe intermetallics were found.

During local anodisation of the Al–Fe alloys using the SDCM, the electric field inside the oxide becomes strong enough so that the activation energy for the ion hopping mechanism was reached [13]. Thus, the beginning of the anodic oxide formation is marked by a sudden increase in the current and the value of the current onset potential (zero current potential – $E_{i=0}$) directly characterises the passivity potential range. It also gives an indication of the thickness of the naturally formed oxide on the surface of the Al–Fe combinatorial library. The dielectric constants of the anodic oxides grown potentiodynamically at up to 10 V on the Al–Fe compositional spread were investigated for different concentrations of the parent alloys in a previous report [7]. Figure 3 shows the OCP and $E_{i=0}$ measured along the sample as a function of the dielectric constant of the anodic oxide. Both curves are presented as nonlinear least square fits to Lorentz distribution functions. The Fe concentrations of the metallic alloys are given in correlation to the permittivity of the corresponding anodic oxides.

The OCP initially increases slowly starting from the value measured on pure Al [approximately −0.18 V as reported to the standard hydrogen electrode (SHE)]. For the permittivity range between 18 and 22, the OCP increases rapidly to a final anodic value of 0.35 V SHE, which does not further change with increasing permittivity up to 25. This plateau suggests a constant surface energy, which can be confirmed by the local microstructure stability observed in Fig. 1 at high Fe concentrations. The sigmoid OCP curve has an inflection point for a dielectric constant value of 19.5 which corresponds to a composition of Al-11.8 at.% Fe for the parent alloy. This coincides very well with the threshold observed in the SEM images at Al-12 at.% Fe (Fig. 1). The transition compositional zone can be associated with a percolation threshold in the Al–Fe alloys, in analogy with the idea described earlier for stainless steels [14, 15], which is based on the formation of a three-dimensional network of a minor element in the matrix of a major one. This idea can also explain the change in the XRD diffraction patterns between two different symmetries.

The evolution of the zero current potential shows a different behaviour. A slight increase in the values of $E_{i=0}$ by less than 100 mV is observed for dielectric constants of up to 16. A significant increase of $E_{i=0}$ (by more than 1 V) is found for anodic oxides with permittivities between 17 and 19.5. After reaching a maximum at 19.5 (11.8 at.% Fe), $E_{i=0}$ decreases faster in the beginning, by about 150 mV, and then continues at a constant rate for permittivities higher than 22. The position of the peak observed in the $E_{i=0}$ curve coincides with the inflection point of the OCP curve. This suggests that the transition from fcc to bcc structure of the metal alloys (see Fig. 2), which happens at the percolation threshold, leads to an increase in the thickness of the naturally grown oxide. The observed differences in the native oxide thickness can be directly attributed to local composition differences, since the history is identical for each investigated point of the sample. Pure Al naturally forms a very thin and protective oxide film that directly follows the high field model of oxide formation [16]. Once the percolation threshold is exceeded, which means that a three-dimensional network of Fe atoms is formed within the Al oxide matrix, the increasing Fe content results in a decrease of oxide film thickness. This is a combined synergistic effect of Al passivation and the catalytic effect of accumulating iron in the Al–Fe combinatorial alloys.

The results of the XPS investigations are summarised in Fig. 4 and three different spectra, corresponding to different parent metal compositions, are shown for O, Fe and Al. For various parent metal compositions, the O 1s peak can always be observed on the surface of the anodic oxide. The spectra recorded for both Al and Fe, show the coexistence of their

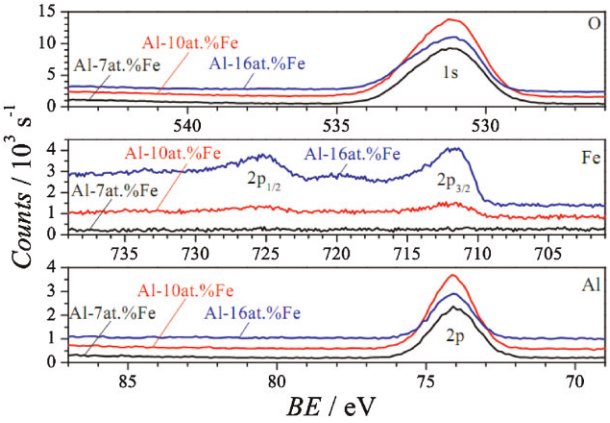

Figure 4 (online colour at: www.pss-a.com) XPS spectra of the anodised Al–Fe alloys measured for three different parent metal compositions.

oxides in the anodised film. The approximate values for the Al and Fe electron affinities are 0.43 and 0.15 eV, respectively. The presence of Al^{3+} was found in all spectra. Only for low concentrations of Fe (Al-7 at.% Fe), no oxidised Fe could be detected on the surface of the mixed anodic oxide. This can be due to the accumulation of the Fe under the oxide film prior to its oxidation [2]. For higher Fe concentrations, the Fe_2O_3 was detected and the XPS peaks were sufficiently intense for allowing a quantitative evaluation. The precise stoichiometry can not be accurately predicted due to the relatively large spread of the peak position corresponding to the Fe_3O_4 (708.2–710.4 eV), which is almost overlapping the Fe^{3+} peak normally found at 710.9 eV [17]. In the present case though, the peak position is slightly higher than 711 eV, most likely due to surface charging, which suggests that Fe^{3+} is the most probable stoichiometry. The concentrations of O found in the anodic oxides, obtained from the integration of the XPS data, were 59, 58.8 and 55 at.%, for Fe concentrations in the alloys of 7, 10 and 16 at.%, respectively. If alumina only can appear as Al_2O_3, the Fe can have various stoichiometries in the oxidised form. Judging by the amount of oxygen found in the mixed oxide, the small deviations of these values from 60 at.% indicate that the amount of Fe in the oxidised state respects the stoichiometry of Fe_2O_3. In this case, the complete mixing of the two individual oxides becomes clear. At the same time, at high Fe concentrations the iron oxide stoichiometry could be Fe_3O_4 since the amount of oxygen needed in this case is 57 at.%. This seems also possible, since the chemical shift of the XPS peaks is below 1 eV. However, the amount measured accounts only partially to Fe (16%), and this would lead more towards concluding that the FeO is present (50 at.% O) for decreasing the total amount of oxygen. In that case a chemical shift of almost 2 eV towards lower energies should have been observed, which is not the case.

The compositions of the mixed anodic oxides were calculated and the results are summarised in Table 1. The

Table 1 Compositions of the mixed anodic oxides as obtained from the XPS quantitative analysis.

Al_{Me}:Fe_{Me} (at.%)	Al_{Ox}:Fe_{Ox} (at.%)	$\Delta^{Me;Ox}$ Al (%)	$\Delta^{Me;Ox}$ Fe (%)
93:7	100:0	+7.5	−100
90:10	96.0:4.0	+6.7	−60.0
84:16	81.2:18.8	−3.3	+17.5

Al_2O_3 to Fe_2O_3 ratios shown in the second column are compared with the corresponding compositions of the parent metal alloys presented in the first column. Also, the deviations of the mixed oxides' compositions as reported to the parent alloys are shown in the last two columns for Al and Fe, respectively. For concentrations of Fe lower than 12 at.%, in the first compositional zone of the alloys, the mixed anodic oxide shows an increase of oxidised Al with more than 5% combined with a dramatically decreased amount of oxidised Fe. Once the percolation threshold in the metallic alloy is reached the composition of the surface oxide changes. For 16 at.% Fe in the parent alloy, a decrease in the amount of the oxidised Al and an increase with 17.5% in the oxidised Fe can be observed. The sudden enrichment of the Fe_2O_3 on the surface of the mixed oxide can be attributed to the faster outward migration of Fe ions as compared with Al ions [2]. The percolation threshold is most likely related with the initial accumulation of Fe under the anodic oxide observed in previous studies [3, 7].

4 Summary In conclusion, the microstructure of an Al–Fe thin film combinatorial library obtained using a co-evaporation technique was analysed. The alloys' surfaces were scanned both along the spatial dimensions of the library and with the potential using an SDCM. All the properties mapped along the concentration gradient showed a similar trend. The SEM and XRD investigations suggested the presence of a transitional region between two metastable phases in the Al–Fe alloys. The transitional zone was marked by the identification of a percolation threshold near Al-12 at.% Fe in the OCP scans which was also found in the mapping of the surface zero current potentials. XPS investigations suggested an intimate mixing of Al_2O_3 and Fe_2O_3 in the anodic oxides. The compositions of the mixed anodic oxides differ from those of the parent alloys and the percolation threshold produced a compositional threshold on the surface of the mixed oxides.

References

[1] T. Mukai, S. Suresh, K. Kita, H. Sasaki, N. Kobayashi, K. Higashi, and A. Inoue, Acta Mater. **51**, 4197–4208 (2003).
[2] H. Habazaki, K. Shimizu, P. Skeldon, G. E. Thompson, and G. C. Wood, Corros. Sci. **43**, 1393–1402 (2001).
[3] H. Habazaki, K. Takahiro, S. Yamaguchi, K. Shimizu, P. Skeldon, G. E. Thompson, and G. C. Wood, J. Electrochem. Soc. **146**, 2502–2507 (1999).

[4] L. M. Prudêncio, I. D. Nogueira, J. C. Waerenborgh, A. P. Goncalves, O. Conde, and R. C. da Silva, Surf. Coat. Technol. **158-159**, 339–342 (2002).
[5] J. Vander Kloet, A. W. Hassel, and M. Stratmann, Z. Phys. Chem. **219**, 1505–1518 (2005).
[6] S. O. Klemm, J. P. Kollender, and A. W. Hassel, Corros. Sci. **53**, 1–6 (2011).
[7] A. I. Mardare, A. P. Yadav, A. D. Wieck, M. Stratmann, and A. W. Hassel, Sci. Technol. Adv. Mater. **9**, 035009-9 (2008).
[8] A. W. Hassel and M. M. Lohrengel, Electrochim. Acta **42**, 3327–3333 (1997).
[9] K. A. Lill and A. W. Hassel, J. Solid State Electrochem. **10**, 941–946 (2006).
[10] M. M. Lohrengel, A. Moehring, and M. Pilaski, Electrochim. Acta **47**, 137–141 (2001).
[11] A. I. Mardare A. D. Wieck, A. W. Hassel. Electrochim. Acta **52**, 7865–7869 (2007).
[12] O. Kubaschewski, Iron-Binary Phase Diagrams (Springer-Verlag, Berlin, 1982).
[13] M. M. Lohrengel, Mater. Sci. Eng. R **11**, 243–294 (1993).
[14] K. Sieradzki and R. C. Newman, J. Electrochem. Soc. **133**, 1979–1980 (1986).
[15] S. Fujimoto, R. C. Newman, G. S. Smith, S. P. Kaye, Kheyrandish, and J. S. Colligon, Corros. Sci. **35**, 51–55 (1993).
[16] A. W. Hassel and M. M. Lohrengel, Mater. Sci. Forum **185**, 581 (1995).
[17] J. F. Moulder, W. F. Stickle, P. E. Sobol, and K. D. Bomben, Handbook of X-ray Photoelectron Spectroscopy, edited by J. Chastain and R. C. King, Jr. (Physical Electronics Inc., Eden Prairie, MN, 1995).